Journal Pre-proof

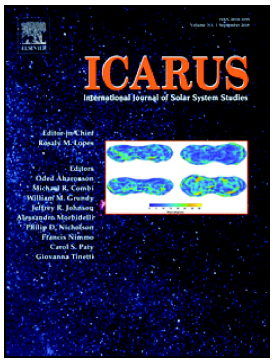

Global thermodynamic, transport-property and dynamic characteristics of the Venus lower atmosphere below the cloud layer

Stefano Morellina, Josette Bellancor, James Cutts

PII: S0019-1035(20)30149-4

DOI: https://doi.org/10.1016/j.icarus.2020.113761

Reference: YICAR 113761

To appear in: *Icarus*

Received date: 5 December 2019

Revised date: 14 February 2020

Accepted date: 16 March 2020

Please cite this article as: S. Morellina, J. Bellancor and J. Cutts, Global thermodynamic, transport-property and dynamic characteristics of the Venus lower atmosphere below the cloud layer, *Icarus* (2018), https://doi.org/10.1016/j.icarus.2020.113761

Global thermodynamic, transport-property and dynamic characteristics of the Venus lower atmosphere below the cloud layer

Stefano Morellina [a], Josette Bellancor [a,b,*], James Cutts [a]

[a] *Jet Propulsion Laboratory, California Institute of Technology, Pasadena, CA 91109, USA*

[b] *California Institute of Technology, Pasadena, CA 91125, USA*

* Corresponding author. Josette.Bellan@jpl.nasa.gov; Tel: (818) 354-6959, Fax: (818) 393-6682.

Abstract

This study investigates the global characteristics of the Venus lower atmosphere below the cloud layer. Starting from available data regarding species composition, temperature and pressure, the general thermodynamic and transport properties of the Venus lower atmosphere are first computed at altitudes below the cloud layer. The thermodynamic and transport properties are validated with known data. A thermodynamic stability analysis for a variety of potentially existing mixtures is conducted to highlight the sensitivity of the thermodynamic regime to the variation of the species molar fractions. The limits of thermodynamic stability are represented in the thermodynamic phase diagram of the mixture, and thus regions of phase stability and instability are determined. It is found that the Venus lower-atmosphere thermodynamic regime is located in the stable, single-phase regime, with supercritical conditions occurring in the lower few kilometers, thereby validating ad-hoc expectations which have never envisaged the existence of a two-phase regime at those altitudes. Using thermodynamic and transport-property information thus computed, several non-dimensional numbers are calculated. The Prandtl number is first evaluated. Then, the characteristic Reynolds number is estimated for different assumed length scales, showing that, independent of the length scale, the entire lower atmosphere below the cloud deck is in a fully-turbulent flow regime. Finally, the speed of sound and the Mach number are computed as function of altitude. The information obtained from all these calculations fills a scientific void, and may be crucial for the design of landers on the Venus surface.

Key words: thermodynamic regime, transport properties and dynamic characteristics of the Venus lower atmosphere

1 Introduction

Venus, the hottest planet in the Solar System, is still subject of intense research. Indeed, and despite the information obtained from several missions conducted to explore the planet, several aspects of its atmosphere remain poorly understood (e.g. Johnson and de Oliveira, 2019, Jacobson et al., 2017, Esposito et al., 2013). For example, the origin of the variety of the chemical species detected close to the Venus surface – within ~ 50 km of altitude – is still unknown as these chemical species could emanate from the Venus solid surface, be the product of local chemical reactions or be transported from upper layers of the atmosphere, particularly from the cloud tops (e.g. Taylor et al., 2018).

There is currently uncertainty as to the origin of the super-rotation, but fluid dynamic principles describing fluid flow in the presence of a surface imply that one of the factors in the establishment of the super-rotation may have been the interaction between the Venus surface and the Venus lower atmosphere occurring in the Venus Planetary Boundary Layer (PBL), a belief already expressed in the literature (e.g. Lebonnois et al., 2018); the PBL is itself coupled to the planet's upper troposphere and tropopause. Thus, understanding the Venus PBL must crucially be addressed as part of the Venus exploration. Understanding the PBL necessarily implies that the characteristics in the lower Venus atmosphere, below the cloud layer, must be understood. However, the presence of sulfuric acid clouds prevent the direct observation of the planet thus requiring special instrumentation (Taylor et al., 2018), and on the other hand the extreme thermodynamic conditions in the lower layers challenge robotic exploration (e.g. Landis and Mellott, 2007). Despite these difficulties, space missions during the last decades have collected a large amount of Venus data, allowing the building of reference models for the Venus atmosphere. Nevertheless, the interpretation of many phenomena is still unclear, and several topics, such as the species stratificatio,n are still open to debate in the scientific community (Lebonnois and Schubert, 2017; Limaye et al., 2018; Cordier et al., 2019).

The purpose of this study is to explore and highlight some of the important aspects of the Venus lower atmosphere and their dependence upon altitude. The interest in investigating the Venus atmosphere characteristics is not new (e.g. Seiff, 1985), but often poor attention is given to the models used to describe the behavior of a multi-species mixture which may be under supercritical conditions. To the best of our knowledge (i) the fluid flow in the Venus lower atmosphere is assumed to be turbulent, but to date the magnitude of the Reynolds number, which is a measure of how turbulent a flow is, has not been determined and (ii) there is wide expectation that the fluid is in the single-phase regime, but no thermodynamic calculation has been made to verify that this is indeed the case.

The study presented here is only the initial step towards developing a rigorous three-dimensional, time dependent model of the Venus atmosphere. Starting from available data regarding the chemical composition of the atmosphere, pressure and temperature values at different altitudes, we first compute in Section 2 atmospheric properties such as density (Section 2.1) and the thermodynamic phase diagram (Section 2.2) that permits considerations of thermodynamic stability. Further, we compute transport properties such as viscosity (Section 3.1) and thermal conductivity (Section 3.2) which allows an evaluation of the characteristic Prandtl number (Section 3.3) as a function of altitude. Further, in Section 4, using published information on lower atmosphere wind speed values, global Reynolds number values are calculated as a function of altitude. Furthermore, the speed of sound and the Mach number as a function of altitude are also computed. Finally, a summary and conclusions are offered in Section 5, and some

of the future studies are outlined.

2 Global thermodynamic characteristics of the Venus lower atmosphere

The information provided in Jacobson et al., 2017 summarizes data from several Venus missions and indicates that in the lower atmosphere, the most preponderant chemical species are those listed in Table 1, where their molar fraction, X_α (α labels a chemical species), thermodynamic critical pressure, p_c, and thermodynamic critical temperature, T_c, and the acentric factor, Ω_α, are provided. At the Venus surface, defined by the altitude $H = 0$ m, the nominal pressure is $p =$ 92 bar and the nominal temperature is $T =$ 735 K (Blumenthal et al., 2012).

Of note, noble gases are not part of the species listed Table 1 Indeed, in a recent paper (Johnson and de Oliveira, 2019) noble gases are listed in the composition of the lower atmosphere but in the Jacobson et al., 2017 study that served to select here the species to be considered, noble gases were only listed as being present but the altitude is not provided. Additionally, no mention of noble gases is made in the overview of de Bergh et al., 2006. Moreover, figure 4 in Baines et al., 2013 shows that the information is only available for Neon and Argon, that for Krypton the information is only known to a factor of 230 and that for Xenon there is absolutely no information. The lack of knowledge regarding the mole fraction of all noble gases combined with their lack of reactivity induced us to relegate their consideration to a future study.

Species	X_α	p_c [bar]	T_c [K]	m_α [kg/kmol]	Ω_α
CO_2	0.9s64816395	73.74	304.12	44.01	0.225
N_2	0.035	33.98	126.2	28.01	0.039
SO_2	0.00015	78.84	430.8	64.07	0.256
H_2O	0.00003	220.64	647.14	18.02	0.344
H_2S	$3x10^{-6}$	89.63	373.4	34.1	0.09
HCl	$6x10^{-7}$	83.1	324.69	36.46	0.133
HF	$5x10^{-9}$	65.0	461.0	20.01	0.329

Table 1: 7-species model for the Venus lower atmosphere (Jacobson et al., 2017). The critical pressure and temperature conditions for the species are listed, as well as their acentric factor (Poling et al., 2001).

2.1 Mixture density

For a mixture of species, the thermodynamic state is completely defined by p, T, X_α and density ρ or equivalently the molar volume v where $v = m/\rho$ where $m = \sum_{\gamma=1}^{N} m_\gamma X_\gamma$ with m_γ being the species molar mass, also listed in Table 1, and N is the number of species. These four quantities are related by the Equation of State (EoS). Generally, the perfect-gas EoS, i.e. $p = \rho R_u T$, is widely used in most applications, but this equation is not necessarily accurate to describe the evolution of the thermodynamic variables in fluids at high p for situations in which the fluid could be in a supercritical state. A supercritical fluid is a pure substance or a mixture of species at (T, p) conditions above its critical point, where there is no distinction between liquid and gas phases (Reid et al., 1987). Such fluids exhibit real-gas behavior.

Depending on the altitude in the Venus lower atmosphere, most of the individual species forming the fluid mixture are in supercritical conditions (refer to Table 1); thus, it is prudent to use a real-gas EoS for computing ρ. For computational efficiency and good accuracy for a variety of species, the cubic Peng-Robinson EoS (PR-EoS) (Reid et al., 1987)

$$p = \frac{R_u T}{(v_{pr} - b_{mix})} - \frac{a_{mix}}{(v_{pr}^2 + 2 b_{mix} v_{pr} - b_{mix}^2)} \tag{1}$$

was selected for this computation. In Eq. (1) $R_u = 8.314$ [J/(mol K)] is the universal gas constant, v_{pr} is the molar PR volume, and a_{mix} and b_{mix} are functions of T and as shown in Appendix A. The accuracy of the PR-EoS has been extensively checked (Harstad et al., 1997; Castiglioni and Bellan, 2018; Gnanaskandan and Bellan, 2018). In those studies, a volume-shift correction was used to enhance the PR-EoS accuracy for those particular species and mixtures of species, whereas in the present study it was verified that random inputs of this volume-shift correction for the minor (i.e. trace) species made no difference in the predictions, meaning that the volume-shift correction is negligible for the minor species in the specific mixtures used here.

Once the PR-EoS is solved for the mixture molar volume v_{pr}, the mixture mass density is easily obtained from

$$\rho = \frac{m}{v_{pr}} \tag{2}$$

where ρ is in [kg/m^3]. Typically, the roots of a cubic EoS are computed by expressing the EoS in terms of the compressibility factor Z (Tester and Modell, 1997)

$$Z^3 + p_1 Z^2 + p_2 Z + p_3 = 0 \tag{3}$$

and when multiple real roots are present, the smallest root corresponds to the liquid root, the middle root is considered unstable and is discarded, and the largest root corresponds to the vapor. The values of the molar mass, molar volume and density obtained for the 7-species mixture (Table 1) at the p = 92 bar and T = 735 K, are summarized in Table 2.

Mixture molar mass, m $[kg/kmol]$	43.4523
Mixture compressibility factor, Z	1.0095

Mixture molar volume, v $[m^3/kmol]$	0.6706
Mixture density, ρ $[kg/m^3]$	64.7972

Table 2: Mixture molar mass, compressibility factor, molar volume and density computed by solving the PR-EOS for p = 92 bar and T = 735 K and the composition listed in Table 1.

The first observation is that $Z \simeq 1$ showing that the mixture has a near perfect-gas behavior (the same result was found by Lebonnois and Schubert, 2017). Further computations up to 65 km show similar results to those obtained with coarser models already present in literature (Seiff, 1985). The preliminary indication is that a perfect-gas model would provide a rough estimate of the mixture thermodynamics. However, since thermodynamics and multi-species transport properties are non-linearly coupled and intertwined (Harstad and Bellan, 2004; Masi et al., 2013), the preliminary indication does not imply that a perfect-gas model could be used in detailed spatio-temporal calculations of species mixing; indeed, the hallmark of non-linearity is that small changes in one variable of the non-linear model may induce large changes in another variable of that model. The form of the mass-diffusion fluxes (Masi et al., 2013; Sciacovelli and Bellan, 2019; Cordier et al., 2019) shows that molecular processes are completely intertwined with thermodynamics (i.e. information from the EoS) and dynamics (i.e. gradients of the dependent variables) so that small departures from perfect-gas or atmospheric-p molecular transport become amplified when there are large dependent-variable gradients (Masi et al., 2013; Sciacovelli and Bellan, 2019), leading to effective transport very different from that obtained for gases at atmospheric p (Masi et al., 2013).

A more refined evaluation on the ρ value is obtained from comparison with the NIST database. Since CO_2 and N_2 represent the preponderant mixture species – over 99.9% in molar fraction – a rough average of ρ values from the NIST database, weighted on Y_α of these species has been performed, and the averaged value was then compared to that computed from the PR-EoS for the 7-species model. Density values compare favorably, as shown in Table 3, showing the excellent reliability of the PR-EoS to model the mixture.

NIST database	Density $\left[kg/m^3\right]$	PR-EOS (7-Species)	error
CO_2	65.894		
N_2	39.808		
$CO_2 - N_2$	65.3078	64.7972	0.8%
mixture			

Table 3: Comparison between the mixture density computed by resolution of the PR-EOS and the density of a mass-fraction-weighted average of a $CO_2 - N_2$ mixture with the species individual values taken from the NIST database. The calculation was performed for p = 92 bar and T = 735 K.

2.2 Thermodynamic regime

The thermodynamic state of a system can be represented in a (p,T,v)-phase diagram in which one identifies two important loci: the binodal and the spinodal. The binodal, or coexistence, locus delineates the single-phase from the two-phase regime. The spinodal separates the thermodynamically-stable regime from the thermodynamically unstable regime. For binary-species systems the metastable regimes (metastable-vapor nucleation and metastable-liquid bubble formation) are located between the binodal and the spinodal, although for mixtures of many species the thermodynamic-phase diagram may have much more complex topology. Metastable states are rare and under the slightest disturbance they degenerate into unstable states (Debenedetti, 1996). The unstable two-phase regime is always found 'under' the spinodal, this region being that to the right of an observer moving on the spinodal in the direction of increasing v. Thus, for all practical purposes the spinodal locus separates stable states from unstable states. Finding the thermodynamic regime of a mixture requires knowing not only (p,T) but also its molar composition, so as to compute v. Whether for a known composition the Venus lower atmosphere is at different altitudes in the single-phase or two-phase regime does matter; for example, if the single-phase regime prevails, this means that 'rain' (drops may have an exotic chemical composition, as compared to the familiar water rain on Earth) is not possible whereas if the two-phase regime prevails this means that 'rain' will occur. Although empirical information indicates that two phases should not be expected, there has not been as of now a scientific evaluation of this expectation.

To compute thermodynamic maps for the Venus lower atmosphere mixture the same methodology adopted and the same validated code in Castiglioni and Bellan, 2018 for calculating the spinodal locus are used. The method has been extensively validated by comparison with experimental data from scientific literature: the critical points for two single species (C_6H_{14} and C_6H_{12}), for two 3-species mixtures ($CH_4/C_6H_{14}/H_2S$; $CH_4/C_6H_{14}/N_2$) respectively for 2 and 4 different compositions, and for one 4-species mixtures ($CH_4/C_6H_{14}/C_2O/H_2S$) for 3 different compositions were calculated using the PR EoS and the results compared excellently with the data. In the present context, to inquire about the sensitivity of the results to the assumed composition (e.g. influence of measurement errors (Jacobson et al., 2017)), the stability analysis is conducted for a variety of mixtures. The mixtures used in computations are selected according to data collected from several Venus observations and missions (Jacobson et al., 2017), and are listed in Table 4. The spinodal loci thus computed are illustrated in Fig. 1 both in the three-dimensional (p,T,v) space and as projections onto the (p,T) and (p,v) planes. Although X_{N_2} is small, clearly the spinodal locus changes both in shape and magnitude according to whether the fluid is portrayed to be CO_2 alone or CO_2 and N_2; however, the presence of the minor species has a negligible impact on the spinodal locus. Projections of the spinodal loci onto the (p,T) and (p,v) planes are also shown in Figs. 2a and 3a to further illustrate the differences between the spinodals computed for CO_2 alone, or CO_2 and N_2. Then, in Figs. 2b and 3b the spinodal loci projections are displayed with enlarged T and v ranges, respectively, to allow the representation of the Venus lower atmosphere at different altitudes and thus to investigate the corresponding thermodynamic regime for the mixtures listed in Table 4. In Fig 2b p is a surrogate for the altitude according to Fig. 4 and in Fig. 3b at each altitude v is computed from PR-EoS, considering the 7-species mixture. In Fig. 3(b) the results are computed with a step of 5 km up to H = 15 km. Both Figs. 2b and 3b show unambiguously that for the known (p,T,X_α) the Venus atmosphere

is always in the stable thermodynamic regime; this conclusion is independent on whether the fluid is assumed to be CO_2, CO_2 and N_2, or the complex multi-species mixtures of Table 4. Eliminating ephemeral metastable states, one can conclude that the Venus lower atmosphere seems to be in a single-phase state and no phase change can be present (e.g. rain). This information is only valid for $H \lesssim 50$ km (Jacobson et al., 2017); at $H \gtrsim 50$ km, where sulfuric acid has been detected, leading to a sulfuric acid haze in the layer immediately below, these results no longer hold.

	1 species	2 species	5 species	7 species	11 species
χ_{CO_2}	1	0.96499	0.96482	0.964816395	0.964693
χ_{N_2}	-	0.03501	0.03500	0.03500	0.03500
χ_{SO_2}	-	-	0.00015	0.00015	0.00015
χ_{H_2O}	-	-	$3x10^{-5}$	$3x10^{-5}$	$3x10^{-5}$
χ_{H_2S}	-	-	$3x10^{-6}$	$3x10^{-6}$	$3x10^{-6}$
χ_{HCl}	-	-	-	$6x10^{-7}$	$6x10^{-7}$
χ_{HF}	-	-	-	$5x10^{-9}$	-
χ_{Ar}	-	-	-	-	$7x10^{-5}$
χ_{CO}	-	-	-	-	$3x10^{-5}$
χ_{He}	-	-	-	-	$1.2x10^{-5}$
χ_{Ne}	-	-	-	-	$7x10^{-6}$
χ_{OCS}	-	-	-	-	$4.4x10^{-6}$

Table 4: Values of X_α for different sets of mixtures used for the Venus lower-atmosphere thermodynamic regime computations.

Fig. 1: Spinodal loci for several mixtures (Table 4) at constant composition, and its projections onto the (p,T) and (p,v) planes.

Fig. 2 : (a) Comparison between spinodal loci for different mixture, onto the (p,T) plane. (b) The Venus lower atmosphere regime is highlighted on the thermodynamic phase diagram, where spinodal loci of Venus-like lower atmosphere mixtures are shown.

Fig. 3: (a) Comparison between spinodal loci for different mixtures, onto the (p,v) plane. (b) Pressure and molar volume conditions in the Venus lower atmosphere are shown for various heights, *H*, on the thermodynamic phase diagram, where spinodal loci of Venus-like lower atmosphere mixtures are shown.

The present thermodynamic phase diagrams are entirely consistent with the information presented in Goos et al., 2011 and with the data of Ke and Poliakoff, 2005; data for the CO_2/N_2 system can also be found in Gernert and Span, 2016.

Thus, while existing Venus observations empirically lead to no expectations of a two phase flow (e.g. rain) in the Venus lower atmosphere, we believe that the present results provide the first model confirmation that such phenomena do not occur in the Venus lower atmosphere for the composition of Table 4 and the *p* and *T* altitude distributions shown in Fig. 4. The absence of phase separation into liquid and gas is here obtained from thermodynamic considerations that address equilibrium states. The present results have no implications for species separation, a topic which can only be addressed by solving time-dependent three-dimensional differential equations involving species-mass diffusion, heat transfer and convective effects. Past studies have proposed that the Venus lower atmosphere is stratified according to altitude (Lebonnois and Schubert, 2017; Limaye et al., 2018), but no fundamental-physics formulation has been proposed that has the ability, now or in the future, to verify this hypothesis through simulations. Proposing such a formulation will not only answer these pending questions but will ultimately have the ability to study the Venus PBL, the super-rotation and to develop estimates of the torque exerted on the planet by the atmosphere; in turn, such estimates could be compared with changes in the length of the day and thereby determine the moment of inertia of the planet. The present investigation is the precursor to those more complex models, simulations and analysis which are deferred to a future study.

3 Global transport properties

Molecular transport at high *p* essentially differs from that at Earth atmospheric *p* in that in the former case molecules are tightly packed so that collisions primarily occur among several molecules whereas in the latter case molecules are far apart so that collisions occur predominantly between two molecules. Since molecular transport properties result from collisional processes, it is expected that quantitative values will be different at high *p* from Earth atmospheric *p*.

Although it would be expedient to compute transport properties based on a CO_2/N_2 mixture, it is shown below that trace species can also be included in these computations. Indeed, trace species may have for some property calculations a disproportionate importance with respect to their X_α values (Sciacovelli and Bellan, 2019), and the goal is here to use a general methodology to account for their specific properties should mission data reveal that either the currently used X_α values require modification, or that new species in the lower Venus atmosphere are discovered. Inherent in the proposed methodology is the comparison with National Institute of Standards and Technology (NIST) data, to evaluate the models.

3.1 Calculation and validation of the mixture viscosity

To compute the individual species viscosity, μ_α, the Lucas method (Reid et al., 1987) has been selected due to its high-*p*-accuracy capabilities. The procedure is to first compute the individual species viscosities and then to use mixing rules to combine the species viscosities to calculate the mixture viscosity. The individual species viscosities are functions of $T_{c,\alpha}$, $p_{c,\alpha}$, m_α, the critical value of *Z*, $Z_{c,\alpha}$, the dipole moment, a high-*p* correction for polarity and actual values of *T* and *p* at which the value of μ_α is desired; the details are shown in Appendix B. To compute the mixture viscosity, μ, the Wilke method (Reid et al., 1987) is used providing:

$$\mu = \sum_{\alpha=1}^{N} X_\alpha \omega_\alpha^M \mu_\alpha \tag{4}$$

$$\left(\omega_\alpha^M\right)^{-1} = \sum_{\beta=1}^{N} \phi_{\alpha\beta} X_\beta \tag{5}$$

where

$$\phi_{\alpha\beta} = \frac{\left[1+\left(\mu_\alpha / \mu_\beta\right)^{1/2}\left(m_\beta / m_\alpha\right)^{1/4}\right]^2}{\left[8\left(1+m_\alpha / m_\beta\right)\right]^{1/2}} \tag{6}$$

in which ω_α^M are weighting factors (Reid et al., 1987), where superscript *M* refers to a quantity related to viscosity.

A comparison between the viscosity value obtained following the Lucas-Wilke methods and that from NIST database is shown in Table 5. Because CO_2 and N_2 constitute the overwhelming composition of the mixture, the NIST viscosity values were weighted by Y_α and the average value was then compared to that computed from Lucas-Wilke methods for the 7-species model. As shown in Table 5, the NIST-computed values compare favorably with the Lucas-method calculation.

NIST database	Viscosity $[Pa \cdot s]$	Lucas-Wilke method (7-Species)	Error
CO_2	3.3476 x 10^{-5}		
N_2	3.4570 x 10^{-5}		
$CO_2 - N_2$	3.3493 x 10^{-5}	3.4546 x 10^{-5}	3.0%
mixture			

Table 5: Comparison between the mixture viscosity computed following the Lucas-Wilke method and the viscosity of a mass-fraction-weighted average of a $CO_2 - N_2$ mixture with the species individual values taken from the NIST database. All calculations were performed for p = 92 bar and T = 735 K. The 7-species mixture is that listed in Table 1.

3.2 Calculation and validation of the mixture molecular thermal conductivity

The individual species molecular thermal conductivity, λ_α, has been computed for each component of the mixture, using the Stiel-Thodos method (Reid et al., 1987; Harstad and Bellan, 2011); the details are described in Appendix C. To summarize, the computation of λ_α uses the reduced density ρ/ρ_c, p_c, T_c, m_α, the acentric factor ω_α and the perfect-gas heat capacities.

Once the λ_α are known, the mixture molecular thermal conductivity is computed following the Wassiljewa-Mason-Saxena method (Poling et al., 2001):

$$\lambda = \sum_{\alpha=1}^{N} X_\alpha \omega_\alpha^Q \lambda_\alpha \tag{7}$$

where superscript Q refers to a quantity related to thermal conductivity, and according to the assumption made by Reid et al., 1987,

$$\omega_\alpha^Q = \omega_\alpha^M . \tag{8}$$

The value of λ computed following Eq. (7) is then compared to a value obtained from the NIST database, in the same manner as for ρ and μ (refer to Tables 3 and 5); the comparison is shown in Table 6.

NIST database	Thermal Conductivity	Wassiljewa-Mason-Saxena	Error
	$[W/(m\cdot K)]$	$[W/(m\cdot K)]$	
CO_2	0.05388		
N_2	0.05313		
CO_2-N_2	0.05385	(7 species) 0.05856	8.0%
mixture			

Table 6: Comparison between the mixture molecular thermal conductivity computed following the Wassiljewa-Mason-Saxena method and the molecular thermal conductivity of a mass-fraction-weighted average of a CO_2-N_2 mixture with the species individual values taken from the NIST database. All calculations were performed for p = 92 bar and T = 735 K. The 7-species mixture is that listed in Table 1.

3.3 Calculation of the mixture Prandtl number

Thermal control of landers on the Venus surface must be carefully engineered to withstand the harsh conditions expected there. One important quantity informing about the momentum diffusivity versus thermal diffusivity is the Prandtl number, Pr. The Prandtl number is defined as

$$\mathrm{Pr} = \frac{C_p \mu}{\lambda} \tag{9}$$

where μ is the viscosity [Pa s], C_p the specific isobaric heat capacity [J/(kg K)], λ is the

thermal conductivity [W/(m K)]. Pr contains no length scale in its definition, and is dependent only on the fluid and the fluid state. Additional to μ and λ, the specific heat capacity, C_p is necessary to compute Pr. Computation of C_p from the EoS involves calculation of derivatives, leading to error accumulation, and therefore this is not the route taken here. Instead, for the 2-species CO_2 and N_2 mixture, the NIST values at $p = 92$ bar and $T = 735$ K are used to compute a Y_α – averaged C_p of the mixture. This value is used, in conjunction with the equivalent NIST-obtained μ and λ found above for the 2-species mixture, to compute Pr; the value thus found is listed in Table 7. To understand the uncertainty in the value of Pr, another calculation is performed for a 7-species mixture employing the $C_p(T)$ expressions of Eq. (C.5), a Y_α -weighted average among the 7 individual species and the μ and λ calculated for 7 species employing the Lucas-Wilke and Wassiljewa-Mason-Saxena methods, respectively. The comparison with the NIST database is shown in Table 7.

Pr (7 species, Lucas-Wilke method/Wassiljewa et al. (Poling et al., 2001))	0.6710
Pr (2 species, data from NIST database)	0.7350
Error	8.7%

Table 7: Comparison between the mixture molecular Prandtl number computed (i) following the Lucas-Wilke and the Wassiljewa-Mason-Saxena methods and (ii) obtaining the mass-fraction-weighted average of a CO_2–N_2 mixture with the species individual values of viscosity, thermal conductivity, and specific heat capacity taken from the NIST database. All calculations were performed for $p = 92$ bar and $T = 735$ K. For the 7-species model, for each species C_p was computed according to Eq. C.5 and the mixture C_p was obtained by mass-fraction averaging where the composition is that of Table 1. For the 2-species mixture, the C_p values at the T and p conditions were used to obtain the C_p value for the mixture by mass-fraction averaging.

Using the same methodology, the Pr value is further computed as a function of altitude by considering the (p,T) variation in Eq. (9) of quantities in the lower 65 km altitude of the atmosphere. Data regarding the variation of T and p with altitude are from Venera 8-12 and Pioneer Venus missions (Seiff, 1983), and are displayed in Fig. 4; these compare favorably with data computed from models (Seiff, 1985; Limaye et al., 2018; Blumenthal et al., 2012). Using these data, C_p, μ and λ of the 7-species mixture are computed for each altitude with a step of 5 km, following the methodology used above. The results are exhibited in Fig. 5 for the ρ, μ, λ and Pr for the 7-species mixture.

Fig. 4: Pressure and temperature variation with altitude in the Venus lower atmosphere (Seiff, 1983; Blumenthal et al., 2012).

Fig. 5: Variation with altitude in the Venus lower atmosphere of (a) ρ, (b) μ, (c) λ (c) and (d) Pr. The computations are performed using the 7-species model, with (p,T) conditions varying with a 5 km step. In particular the $C_p(T)$ model of Eq. (C.5) is used.

As it is apparent, Pr has an approximately 3% variation with altitude through the Venus lower atmosphere. This information means that a lander will not be exposed during Venus-surface descent to a flow having large Pr variations. Because $\mathrm{Pr}<1$, this means that the thermal boundary layer on a lander will be thicker than the momentum boundary layer and that heat diffuses quickly compared to the velocity (momentum), all of which are useful considerations for thermal control. Indeed, heat transfer with the environment is important in determining the useful lifetime of a Venus-surface lander. The interior temperature of the lander is set by design to be close to terrestrial room temperatures (300 K), and may not change substantially during Venus descent. As the spacecraft rests on the surface, heat diffuses into it (the process is enhanced by turbulence; see Section 4.1) through its insulating shell and this process also depends on the Pr value; additionally, the internal temperature will also rise because of internal heat generation as a result of power consumed by the instruments and communication systems. The internal temperature rise is conceivable to be modulated by the use of a phase change material using either a solid/liquid phase transition (e.g. lithium niobate) which melts at 303 K or utilizing a liquid/vapor transition such as ammonia; these are prospective concepts, so far unimplemented. In the latter case, the vapor must be released to the environment which typically would occur at 383 K; this process will also be impacted by the Pr value.

4 Global dynamic characteristics

Turbulence in a medium is characterized by the Reynolds number, Re, and sound propagation in a medium is characterized by the speed of sound, a_s, from which the Mach number, *Ma*, is usually computed. These numbers are property of a flow of a given composition and at specified (p,T) conditions. As such they are quantities of scientific interest for the understanding of the Venus atmosphere, as well as of interest for engineers making decisions on lander design.

4.1 Calculation of the Reynolds number

The Reynolds number is defined as

$$\mathrm{Re} = \frac{\rho V L}{\mu} \tag{10}$$

where ρ, V, L and μ are characteristic values of density, velocity magnitude, length scale and viscosity. Re represents the ratio between the inertial and the viscous forces, thus being a good metric in determining whether a flow is laminar ($\mathrm{Re} \lesssim O(10^2) - O(10^3)$) or turbulent ($\mathrm{Re} \gtrsim O(10^3) - O(10^5)$). The boundary between laminar and turbulent flow is not firm and there is an intermediary regime in which a flow is transitioning from one regime to the other. The achievement of turbulent transition is recognized by the fact that the fluctuation-based spectra of

the dependent variables (i.e. velocity, species mass fractions and temperature) versus the wavenumber k (units of m^{-1}) exhibit a smooth aspect, signifying that the characteristic turbulent regime in which there is a continuum of scales has been reached.

To find characteristic values to compute Re we look for Venus-observation data. The available information reveals that winds near the Venus surface have a much smaller value than that on the upper atmosphere, where the super-rotation phenomenon occurs; direct and indirect measurements showed that these winds have a velocity of only a few kilometers per hour, with an average of 0.3 to 1.0 m/s (Basilevsky and Head, 2003; Moshkin et al., 1979). A mean profile of the zonal (east-to-west) wind on Venus as measured by tracking the Pioneer Venus entry probes have been taken into account (Bengtsson et al., 2013) in illustrating V in Fig. 6a.

There is difficulty in making an educated choice regarding a characteristic length scale for dynamic processes. Visible images from surface observations show stones and boulders of about 50 cm, as illustrated in Fig. 7a. The top image of Fig. 7a was taken by Venera 9 and the lower one was obtained by Venera 10 (Florensky et al., 1977); these images were obtained on 22 and 25 October 1975. The rocks in the foreground in Venera 9 are about 10 to 20 cm in size, while most rocks in the images have sizes between about 0.3 and 1 meter. A distorted view of the horizon appears at the upper right of both images. On the other hand, radar images of surface from orbit show surface structural elements with a repeat distance of approximately 5 km, as illustrated in Fig. 7b. This image shows the 69 km diameter Dickinson crater (Schaber et al., 1992) which is located at 74.6 North latitude and 177.2 East longitude, in the northeastern Atalanta Region of Venus. The crater is complex, characterized by a partial central ring and a floor flooded by radar-dark and radar-bright materials. Hummocky, rough-textured ejecta extend all around the crater, except to the west. The lack of ejecta to the west may indicate that the impactor that produced the crater was an oblique impact from the west. Extensive radar-bright flows that emanate from the crater's eastern walls may represent large volumes of impact melt, or they may be the result of volcanic material released from the subsurface during the cratering event. Some aspects are stochastic, others are regular. For simulations in the 50 km altitude range of the atmosphere, the interest is in the macrostructure of the surface, so that a first educated choice is $L = 50$ m. The resulting Reynolds number for each altitude, computed by using the Eq. (10) and a characteristic length scale of 50 m is shown in Fig. 6b.

Fig. 6: Variation with altitude in the Venus lower atmosphere of (a) V and (b) Re computed using the velocity profile with altitude, $L = 50$ m and μ computed as a function of altitude for the 7-species mixture.

Fig. 7: Length scales on Venus: (a) Venus surface details from Venera 9 and 10 lander, showing rocks of about 50 cm. (b) The Dickinson crater on Venus as observed by the Magellan orbiter, showing 5 km features.

Considering a flow velocity, V, of 1 m/s and a characteristic length scale, L, of 50 m, the Reynolds number computed with ρ calculated from the PR-EoS and μ using the Lucas-Wilke

method for seven species is shown in Table 8 together with Reynolds number computed using NIST values for two species. The values obtained show a discrepancy of only $\simeq 3\%$, indicating reliability of the model and of the computational procedure. The favorable evaluations shown above provide motivation for obtaining more extended results, according to the value of L; for example, Re values corresponding to L in the meter range would be of interest for aerothermodynamics studies of space probes such as landers and rovers, or for re-entry situations. Figure 8 illustrates Re versus altitude for three different values of L. In all cases, the Re value between 0 km and 65 km indicates a fully-turbulent regime. From the simulation-type viewpoint, this means that to study the macrostructure the entire Venus lower atmosphere with boundaries at 0 km and 50 km, a computational tool appropriate for Re values in the range shown in Fig. 8 must be used. Since Reynolds Average Navier-Stokes methods propose to represent all scales of a physical process by the same model, they are unable to accurately accommodate scale-specific phenomena, and are thus not recommended for Venus atmospheric studies which involve large-scale stirring and small-scale diffusional mixing. Instead, Large-Eddy Simulation (LES) methods in which the large scales are computed and the small scales are modeled should be used, and Direct Numerical Simulation methods wherein all scales are computed in smaller domains and at smaller but relevant Reynolds numbers, should guide the development of the small-scale models needed in LES. This work is relegated to the future.

Reynolds number (7-species, PR-EOS/Lucas-Wilke method)	93783992
Reynolds number (2-species, data from NIST database)	96986657
Error	3.3%

Table 8: Comparison between the Reynolds number computed by resolution of the PR-EOS and following the Lucas-Wilke method and the Reynolds number for a molar mass-weighted average of a CO_2-N_2 mixture with the species individual values of density and viscosity taken from the NIST database . The characteristic length scale and velocity scale used to compute the Reynolds number are the same for both methods.

Figure 8: Reynolds number values at different altitudes according to the selected length scale. The shaded region represents the lower-turbulence regime.

4.2 Calculation of the speed of sound and the Mach number

The knowledge of the speed of sound value, a_s, at the Venus surface is scientifically important because it determines the transmission of seismic energy across the Venus-surface/atmosphere interface. For example, it has been proposed that observations of Venus quakes could be made from platforms floating in the Venus atmosphere (Cutts et al., 2016; Krishnamoorthy et al., 2019); when the difference between the speed of sound in the atmosphere and in the underlying rocks is small, larger amounts of seismic energy are being transmitted into the atmosphere for detection. The knowledge of the a_s gradient with respect to altitude is also important because it controls the refraction of sound waves from the surface that will determine the

path from a seismic event to the observing stations. The a_s value of CO_2, obtained from the NIST database using the (p,T) values correspondent to each altitude (calculations were performed with a 5 km step) is illustrated in Fig. 9a together with the values of a_s at 0.4 km, 10 km and 50 km altitude computed assuming that the lower Venus atmosphere has the 7-species nominal composition listed in Table 4. The error in a_s between the CO_2 and 7-species computed values is 0.9 %, 1.9 % and 0.7 % at the 0.4 km, 10 km and 50 km altitudes.

The knowledge of *V* together with that of a_s, permits the calculation of *Ma*

$$Ma = \frac{V}{a_s}. \tag{11}$$

The variation of the Mach number with altitude is calculated using the *V* information in Fig. 6a and the a_s value from Fig. 9a; the results are depicted in Fig. 9b and show a similar variation to that of the *V* distribution with altitude. Close to the Venus surface, *Ma* is very small, but this does not necessarily signify an incompressible flow since there maybe substantial gradients in velocity, X_α and *T*, all of which may contribute to a substantial irreversible entropy production, i.e. the dissipation (Batchelor, 1999). At an altitude corresponding to the cloud layer, the *Ma* value is still in the subsonic regime. This *Ma* information is crucial in selecting the type of physical model to be used in future three-dimensional time-dependent high-fidelity calculations without parametrization of quantities such as the turbulent diffusivity.

Fig. 9: Distribution of (a) the speed of sound with altitude and (b) the Mach number with altitude in the Venus lower atmosphere. The curves were obtained by assuming that the atmosphere only contains CO_2, whereas the red-color symbols represent calculations performed assuming the 7-species composition of Table Table 4.

5 Summary and conclusions

Venus data from missions or observations have been used to determine the general characteristics of the Venus lower atmosphere below the cloud layer. Utilizing published composition, temperature and pressure at different altitudes, a real-gas equation of state has been used to compute the density, and state-of-the-art models have been used to compute transport properties of the species in the mixture constituting the fluid in the lower atmosphere. The density and transport properties results favorably match those available through the National Institute of Standards and Technology at the same pressure and temperature conditions, and the error depends on the assumptions regarding the mixture composition. Real-gas effects and presence of minor species have minor impact on the compressibility factor which is nearly unity, with a maximum error varying from 1% to 3% with respect to the perfect gas behavior, depending on the mixture composition; this error is perhaps negligible for those applications which require a only a rough value of the density but, because of strong non-linear coupling between thermodynamics and transport (Harstad and Bellan, 2004; Masi et al., 2013), may become substantial in studies

including multi-species mass-diffusion fluxes that would be instrumental in settling the open issue of species stratification.

Furthermore, using the equation of state, the thermodynamic regime of various sets of mixtures, which according to the literature may exist in the Venus atmosphere, has been computed thus highlighting the stability and instabilities regions. The presence of nitrogen in the mixture significantly changes the limit of thermodynamic stability (i.e. the spinodal locus shape), whereas the minor species have negligible influence on the thermodynamic regime. For all nominal Venus lower-atmosphere fluid-mixtures considered, the thermodynamic regime for the realistic pressures and temperatures in the Venus lower atmosphere is located in the stable single-phase regime for the first 65 km, with supercritical conditions occurring in the lower few kilometers. Following thermodynamic theory we have thus verified the empirical expectation that no transient unstable phenomena (e.g. 'rain') can exist in the lower atmosphere of Venus.

From thermodynamic and transport information, the Prandtl number was evaluated as a function of altitude for the specific pressure and temperature conditions. Moreover, employing published data on the wind speed from Venus space missions in conjunction with the computed density and viscosity, the Reynolds number was calculated over macroscopic characteristic length scales as a function of altitude for the specific pressures and temperatures prevailing at those altitudes. For three possible characteristic length scales sequentially increasing by one order of magnitude, the Reynolds number value of the flow was found to be in the fully-turbulent regime for the entire lower atmosphere. Computing the speed of sound from the equation of state and utilizing the published wind speed allowed the calculation of the Mach number as a function of altitude. The Mach number was found to increase with altitude and reach ~ 0.4 at ~ 60 km, as the speed of sound decreases with altitude.

Current interest in Venus missions with landers able to sustain the harsh conditions of the Venus lower atmosphere as far as material integrity is concerned (e.g. melting, corrosion (for modeling reactions under high-pressure turbulent conditions see Bellan, 2017)) make simulations of the Venus lower atmosphere a necessary component of mission design. Additionally, proliferation of experimental facilities for simulating the Venus environment (e.g. Kremic et al., 2016; Lambert et al., 2010) – for the purpose of understanding the effects of species mixing on engineering systems and understanding geological materials reacting under the Venus thermodynamic conditions – is to date unsupported by a theoretical framework. The present study, and the potential it has for performing well-informed physics-based spatio-temporal simulations devoid of calibrated parameters, provides the much needed coupling of the experiment with theory in order to create a concerted effort to develop new science. Additional to the clear scientific knowledge gained by computing the Reynolds number, Prandtl number and Mach number values, their combined knowledge provides valuable information regarding the type of models and appropriate numerical methods to be used in future advanced simulations of these flows that will not rely on parametrizations, as current models do (e.g. Global Circulation models) (Bierson and Zhang, 2019), making it thus impossible to accurately predict the spatial variation of several species. The large value of the Reynolds number means that Large Eddy Simulation is the fluid dynamic model of choice, and the Mach number values smaller than unity indicate that subsonic flow numerical techniques should be used when solving the differential conservation equations; the value of the Prandtl number is indicative as to whether the dynamic scales are smallest ($Pr < 1$) or the thermodynamic scales are smallest ($Pr > 1$) and thus can inform on the necessary resolution of spatio-temporal computations. Additionally, the molecular Prandtl number value, being found here quantitatively similar to that of perfect gas, indicates that should it be found in future spatial

simulations that the effective Prandtl number (Masi et al., 2013) differs from its molecular value, the difference will be attributable to the non-linear coupling among transport properties, thermodynamics and dynamics. Essentially, the present global study will not only inform future spatially-resolved studies, but also enable the interpretation of the results from those forthcoming investigations.

Acknowledgments

This work was conducted at the Jet Propulsion Laboratory (JPL) of the California Institute of Technology (Caltech) and sponsored by JPL internal development funds. This study is part of Stefano Morellina's (SM) Master thesis and was performed while he was an intern at JPL. The contributions of Dr. Aswin Gnanaskandan and Dr. Luca Sciacovelli are thankfully recognized. Stefano Morellina's Master thesis supervisor, Dr. Francesco Creta, and the Co-supervisor, Dr. Pasquale E. Lapenna, are thanked for their advice and for helping SM to find financial support. The Fondation ISAE-SUPAERO, Italian Space Agency and Fondazione Sapienza are thanked for providing financial support to SM during his internship at JPL. The computational resources were provided by the NASA Advanced Supercomputing at Ames Research Center under the Science Mission Directorate program.

Copyright

A Equation of state details

Miscellaneous relationships relevant to the EoS are

$$a_{mix} = \sum_{\alpha}\sum_{\gamma} X_\alpha X_\gamma a_{\alpha\gamma}(T), b_{mix} = \sum_{\alpha} X_\alpha b_\alpha, \tag{A.1}$$

where indices do not follow the Einstein notation, and

$$a_{\alpha\gamma} = (1-k'_{\alpha\gamma})\sqrt{\alpha_{\alpha\alpha}\alpha_{\gamma\gamma}}, \tag{A.2}$$

$$\alpha_{\alpha\alpha}(T) \equiv 0.457236(R_u T_{c,\alpha})^2 \times \frac{\left[1+c_\alpha(1-\sqrt{T_{r,\alpha}})\right]^2}{p_{c,\alpha}}, \tag{A.3}$$

$$c_\alpha = 0.37464 + 1.54226\Omega_\alpha - 0.26992\Omega_\alpha^2, \tag{A.4}$$

where $T_{r,\alpha} \equiv T/T_{c,\alpha}$, $T_{c,\alpha}$ is the critical temperature and Ω_α is the acentric factor (values available from NIST database). Also,

$$b_\alpha = 0.077796 \frac{R_u T_{c,\alpha}}{p_{c,\alpha}}, \tag{A.5}$$

$$T_{c,\alpha\gamma} = \left(1 - k_{\alpha\gamma}\right)\sqrt{T_{c,\alpha} T_{c,\gamma}} \quad \text{with } k_{\alpha\alpha} = 0, \tag{A.6}$$

$$v_{c,\alpha\gamma} = \frac{1}{8}\left(v_{c,\alpha}^{1/3} + v_{c,\gamma}^{1/3}\right)^3, \tag{A.7}$$

$$Z_{c,\alpha\gamma} = \frac{1}{2}\left(Z_{c,\alpha} + Z_{c,\gamma}\right), \tag{A.8}$$

$$p_{c,\alpha\gamma} = \frac{R_u T_{c,\alpha\gamma} Z_{c,\alpha\gamma}}{v_{c,\alpha\gamma n}}, \tag{A.9}$$

with $T_{r,\alpha\gamma} \equiv T / T_{c,\alpha\gamma}, Z_{c,\alpha}$ being the critical compressibility factor with the compressibility factor defined as $Z = p/(\rho T R_u / m)$, $v_{c,\alpha}$ being the critical volume, and $p_{c,\alpha}$ being the critical pressure. $k_{\alpha\gamma}$ is an empirical mixing parameter. The relationship between parameters $k_{\alpha\gamma}$ and $k'_{\alpha\gamma}$ is

$$(1 - k_{\alpha\gamma}) = (1 - k'_{\alpha\gamma}) \frac{(v_{c,\alpha} v_{c,\gamma})^{1/2}}{v_{c,\alpha\gamma}}. \tag{A.10}$$

and for all pairs not in Table 1, $k'_{\alpha\gamma} = 0$ is used.

Species 1	Species 2	k'
CO_2	N_2	-0.017
CO_2	H_2O	0.12
CO_2	H_2S	0.0974
N_2	SO_2	0.08
N_2	H_2S	0.1767
H_2O	H_2S	0.04

Table 1: Binary interaction parameters when the first species has a relatively low molar mass. Parameters not listed are set to be null. The reference is Knapp et al. (1982).

B Species viscosity computation

The individual species viscosity is computed as

$$\mu_\alpha = \frac{Z_2\, F_P}{\xi\, 10^{-7}} \tag{B.1}$$

where μ_α is in $[\mathrm{Pas}]$. The calculation of the coefficients Z_2, F_P, ξ is shown in the following lines.

We define the reduced inverse viscosity as:

$$\xi = 0.176\left(\frac{T_c}{m_\alpha^3 p_c^4}\right)^{1/6} \tag{B.2}$$

where ξ is in $[\mu P]^{-1}$, T_c is in K, m_α is in g/mol, and p_c is in bar.

The correction factor for polarity effect, F_P° is

$$\begin{aligned} F_P^\circ &= 1 && 0 \le dipm_r < 0.022 \\ F_P^\circ &= 1 + 30.55(0.292 - Z_c)^{1.72} && 0.022 \le dipm_r < 0.075 \\ F_P^\circ &= 1 + 30.55(0.292 - Z_c)^{1.72}\,|0.96 + 0.1(T_r - 0.7)| && 0.075 \le dipm_r \end{aligned} \tag{B.3}$$

where Z_c is the critical compressibility factor of the pure species, $dipm_r$ the reduced dipole moment defined as:

$$dipm_r = 52.46\frac{dipm^2\, p_c}{T_c^2} \tag{B.4}$$

$dipm$ being the dipole moment of the species in debye, p_c in bar , and T_c in K.

The effect of high p on viscosity is taken in account using two parameters Z_1 and Z_2:

$$Z_1 = \left[0.807 T_r^{0.618} - 0.357\exp(-0.449 T_r) + 0.340\exp(-4.058 T_r) + 0.018\right] F_P^\circ \tag{B.5}$$

If the reduced values of T and p, $T_r = T/T_c$ and $p_r = p/p_c$, are such that $1 < T_r < 40$ *and* $0 < p_r \le 100$, then

$$\begin{aligned} Z_2 &= Z_1\left[1 + \frac{a p_r^{1.3088}}{b p_r^f + (1 + c p_r^d)^{-1}}\right] \\ &\text{with } a = 1.245\,10^{-3}\frac{5.1726 T_r^{-0.3286}}{T_r}; \qquad d = 1.73\frac{\exp(2.2310 T_r^{-7.6351})}{T_r}; \\ &b = a(1.6553 T_r - 1.2723); \qquad f = 0.9425\exp(-0.1853 T_r^{0.4489}); \\ &c = 0.4489\frac{\exp(3.0578 T_r^{-37.7332})}{T_r} \end{aligned} \tag{B.6}$$

If $T_r \le 1$ *and* $p_r < 1$, then

$$Z_2 = 0.600 + 0.760\,p_r^{\alpha} + (6.990\,p_r^{\beta} - 0.6)(1 - T_r)$$
$$\text{with } \alpha = 3.262 + 14.98\,p_r^{5.508}; \quad \beta = 1.390 + 5.746\,p_r. \tag{B.7}$$

For all other cases of T_r and p_r, $Z_1 = Z_2$ has been assumed. Therefore, the high-*p* correction for polarity is:

$$F_P = \frac{1 + (F_P^{\circ} - 1)\left(\frac{Z_2}{Z_1}\right)^{-3}}{F_P^{\circ}} \tag{B.8}$$

C Species thermal conductivity calculation

$$\lambda_{\alpha} = \lambda_{\alpha}^{0} + \frac{FE_p}{\Gamma Z_{c,\alpha}^{5}} \tag{C.1}$$

Where $Z_{c,\alpha}$ is the critical compressibility factor of the species α, and the coefficients $FE_p, \lambda_{\alpha}^{0}, \Gamma$ are computed as follows:

$$\begin{aligned} FE_p &= 1.22\times10^{-2}[\exp(0.535\rho_r) - 1] && \rho_r < 0.5 \\ FE_p &= 1.14\times10^{-2}[\exp(0.67\rho_r) - 1.069] && 0.5 < \rho_r < 2.0 \\ FE_p &= 2.60\times10^{-3}[\exp(1.155\rho_r) + 2.016] && 2.0 < \rho_r < 2.8 \end{aligned} \tag{C.2}$$

with ρ_r the reduced density $\rho / \rho_c = v_c / v$.

$$\lambda_{\alpha}^{0} = R_u[3.75 + f_{int}(C_p^{\circ} / R_u - 2.5)]\frac{\eta^{\circ}}{m_{\alpha}} \tag{C.3}$$

where, m_{α} is the molar mass of the species in [kg/mol], $R_u = 8.314$ [J/(mol·K)] is the universal gas constant.

$$f_{int} = \frac{1}{0.7862 - 0.7109\omega_\alpha + 1.3168\omega_\alpha^2} \tag{C.4}$$

with ω_α being the acentric factor. The ideal heat capacities for the individual species, C_p° / R_u, is computed as follows:

$$C_p^\circ / R_u = a_0 + a_1 T + a_2 T^2 + a_3 T^3 + a_4 T^4 \tag{C.5}$$

with the constants a_0, a_1, a_2, a_3, a_4 given in Poling et al., 2001 (Appendix A, Section C).

$$\eta^\circ = \frac{Z_1}{\xi 10^{-7}} \tag{C.6}$$

where Eqs. (B.5) and (B.2) are used for Z_1, ξ computation. The reduced, inverse thermal conductivity, Γ,

$$\Gamma = 210\left(\frac{T_c^3 m_\alpha^3}{p_c^4}\right)^{1/6} \tag{C.7}$$

is in $[\mathrm{W/(m \cdot K)}]^{-1}$, T_c is in K, m_α s is in g/mol, and p_c is in bar.

References

Baines K. H., Atreya S. K., Bullock M. A., Grinspoon D. H., Mahaffy P., Russell C. T., Schubert G., Zahnle K. 2013. The atmospheres of the terrestrial planets: Clues to the origins and early evolution of Venus, Earth, and Mars. Comparative Climatology of Terrestrial Planets (S. J. Mackwell et al., eds.), Univ. of Arizona, Tucson, 137–160.

Basilevsky, A. T., Head, J. W., 2003. The surface of Venus. Rep. Prog. Phys. 66, 1699-1734.

Batchelor, G. K., 1999. An Introduction to Fluid Dynamics. Cambridge University Press.

Bellan, J., 2017. Direct numerical simulation of a high-pressure turbulent reacting temporal mixing layer. Combustion and Flame 176, 245–262.

Bengtsson, L., Bonnet, R.M., Grinspoon, D., Koumoutsaris, S., Lebonnois, S., Titov, D., 2013. Towards Understanding the Climate of Venus - Applications of Terrestrial Models to Our Sister Planet. ISSI Scientific report Series.

Bierson, C.J. , Zhang, X., 2019. Chemical cycling in the Venusian atmosphere: A full photochemical model from the surface to 110 km. submitted to Journal of Geophysical Research

Blumenthal, G., Kay, L., Palen, S., Smith, B., 2012. Understanding Our Universe. New York: W.W. Norton & Company. p. 167.

Castiglioni, G., Bellan, J., 2018. On models for predicting thermodynamic regimes in high-pressure turbulent mixing and combustion of multispecies mixtures. J. Fluid Mech. 843, 536-574.

Castiglioni, G., 2018. Personal communication.

Cordier, D., Bonhommeau, D.A., Port, S., Chevrier, V., Lebonnois, S., Garca-Sánchez, F., 2019. The physical origin of the Venus low atmosphere chemical gradient. The Astrophysical Journal, 880-82 (8pp).

Cutts, J. A., Pauken, M., Jackson, J.M., Mimoun, D., 2016 Venus Exploration with Infrasound Techniques, 3rd International Workshop on Instrumentation for Planetary Missions, 4107.

Debenedetti, P. G., 1996. Metastable liquids: concepts and principles. Princeton University Press.

de Bergh, C., Moroz, V.I., Taylor, F.W., Crisp, D., Bézard , B., Zasova, L.V. 2006. The composition of the atmosphere of Venus below 100 km altitude: An overview. Planetary and Space Science, 54, 1389-1397.

Esposito, L.W., Stofan, E. R., Craven, T. E., 2013. Exploring Venus as a Terrestrial Planet, Wiley.

Florensky, C.P., Ronca, L.B., Basilevsky, A.T., Burba, G.A., Nikolaeva, O.V., Pronin, A.A., Trakhtman, A.M., Volkov, V.P., Zazetsky, V.V. 1977. The surface of Venus as revealed by Soviet Venera 9 and 10, Geological Society of America Bulletin, 88 (11), 1537–1545.

Gernert, J., Span, R. 2016. EOS–CG: A Helmholtz energy mixture model for humid gases

and CCS mixtures. J. Chemical Thermodynamics, 93, 274–293.

Gnanaskandan, A., Bellan, J. 2018. Side-jet effects in high-pressure turbulent flows: Direct Numerical Simulation of nitrogen injected into carbon dioxide. J. Supercritical Fluids, 140, 165-181.

Goos, E., Riedel, U., Zhao, L., Blum, L. 2011. Phase diagrams of CO_2 and CO_2-N_2 gas mixtures and their application in compression processes. Energy Procedia 4, 3775-3785.

Harstad, K., Miller, R. S., Bellan, J., 1997. Efficient High-Pressure State Equations, A.I.Ch.E. J., 43(6), 1605-1610.

Harstad, K.G., Bellan, J., 2011. Computation of Laminar Premixed Flames Using Reduced Kinetics Based on Constituents and Species. AIAA-2011-415.

Harstad, K.G., Bellan, J., 2004. Mixing rules for multicomponent mixture mass diffusion coefficients and thermal diffusion factors. J. Chem. Phys. 120(12), 5664–5673.

Jacobson, N. S., Kulis, M., Radoman-Shaw, B., Harvey, R., Myers, D.L., Schaefer, L., Fegley, Jr., B., 2017. Thermodynamic Constraints in the Lower Atmosphere of Venus. ACS Earth and Space Chem. 1,422-430.

Johnson, N. M., de Oliveira, M.R.R., 2019. Venus atmospheric composition in situ data: a compilation. Earth and Space Science 6, 1299–1318.

Ke, J., Poliakoff, M., 2005. The critical point of CO_2 + N_2: an experiment inspired by *Notes and Records* Notes Rec. R. Soc. 59, 171–174.

Knapp, H., Döring, R., Oellrich, L., Plöcker, U., Prausnitz, J.M., 1982. Vapor-liquid Equilibria for Mixtures of Low Boiling Substances, vol VI. Dechma.

Kremic, T.,. Nakley, L., Vento, D., Balcerski, J., Kulis, M. J., Jacobson, N. S. Costa, G. C. C. 2016. Glenn Extreme Environments Rig (GEER) for planetary science, 47th Lunar and Planetary Science Conference, paper 2146

Krishnamoorthy, S., Lai, V.H., Komjathy, A., Pauken, M.T., Cutts, J.A., Garcia, R.F., Mimoun, D., Jackson, J.M., Bowman, D.C., Kassarian, E., Martire, L., Sournac, A., Cadu, A. 2019. Aerial Seismology Using Balloon-Based Barometers. IEEE Transactions on Geoscience and Remote Sensing, 57 (12) 10191-10201.

Lambert, J., Morookian, J., Roberts, T., Polk, J., Smrekar, S., Clegg, S. M., Wiens, R. C., Dyar, M. D., Treiman A., 2010. Standoff LIBS and Raman Spectroscopy under Venus Conditions, 41st Lunar and Planetary Science Conference, paper 2608.

Landis, G. A., Mellott, K.C., 2007. Venus surface power and cooling systems. Acta Astronautica, 61(11-12), 995-1001.

Lebonnois, S., Schubert, G., 2017. The deep atmosphere of Venus and the possible role of density-driven separation of CO_2 and N_2. Nat. Geosci. 10, 473-477.

Lebonnois, S., Schubert, G., Forget, F., Spiga, A., 2018. Planetary boundary layer and slope winds on Venus. Icarus 314, 149-158.

Limaye, S. S., Grassi, D., Mahieux, A., Migliorini, A., Tellmann, S., Titov, D., 2018. Venus atmospheric thermal structure and radiative balance. Space Science Reviews 214 (5) DOI: 10.1007/s11214-018-0525-2.

Masi, E., Bellan, J., Harstad, K.G., Okong'o, N.A., 2013. Multi-species turbulent mixing under supercritical-pressure conditions: modelling, direct numerical simulation and analysis revealing species spinodal decomposition. J. Fluid Mech. 721, 578-626.

Moshkin, B.E., Ekonomov, A.P., Golovin, Iu.M., 1979. Dust on the surface of Venus. Cosmic Research 17, no. 2, Sept., 232-237.

National Institute of Standards and Technology. Website: https://webbook.nist.gov/chemistry/fluid/

Poling, B. E., Prausnitz, J. M., O'Connell, J.P., 2001. The Properties of Gases and Liquids. McGraw-Hill.

Reid, R.C., Prausnitz, J.M., Poling, B.E., 1987. The Properties of Gases and Liquids. 4th

edn. McGraw-Hill.

Schaber, G.G., Strom, R.G., Moore, H.J., Soderblom, L.A. , Kirk, R.L., Chadwick, D.D., Dawson, D.D., Gaddis, L.R., Boyce, J.M., Russell, J. 1992. Geology and distribution of impact craters on Venus: What are they telling us? J. of Geophysical Research, 97(E8), 13,257-13,301.

Sciacovelli, L., Bellan, J. 2019. The influence of the chemical composition representation according to the number of species during mixing in high-pressure turbulent flows. Journal of Fluid Mechanics, 863, 293-340.

Seiff, A. 1983. Thermal structure of the atmosphere of Venus, Venus (D. M. Hunten, L. Colin, T. M. Donahue, and V. I. Moroz, eds.) University of Arizona Press 215-279.

Seiff, A., Schofield, J. T., Kliore, A. J., Taylor, F. W., Limaye, S. S., Revercomb, H. E., Sromovsky, L. A., Kerzhanovich, V. V., Moroz, V. I., Marov, M. Ya.,1985. Models of The Structure of The Atmosphere of Venus from the Surface to 100 kilometers Altitude. Adv. Space Res. 5(11), 3-58.

Taylor, F.W., Svedhem, H., Head III, J.W., 2018. Venus: The atmosphere, climate, surface, interior and near-space environment of an earth-like planet. Space Sci Rev. 214(35), 1-36.

Tester, J.W., Modell, M., 1997. Thermodynamics and its applications. Prentice Hall PTR.

Highlights

- A thermodynamic stability analysis was conducted for the nominal composition, temperature and pressure in the Venus lower atmosphere and it was found that the atmosphere is in the supercritical regime.
- It was found that the thermodynamic stability boundary is different if one assumes the atmosphere to be CO_2 or to be a mixture of CO_2 and N_2, but the stability boundary is insensitive to the addition of Venus lower-atmosphere trace species to the CO_2/N_2 mixture.
- The viscosity and thermal conductivity were computed for the nominal seven-species composition, temperature and pressure of the Venus lower atmosphere.
- The value of the Reynolds number was calculated as a function of the Venus altitude for various characteristic lengths.
- The speed of sound and the Mach number were calculated as a function of the Venus altitude.

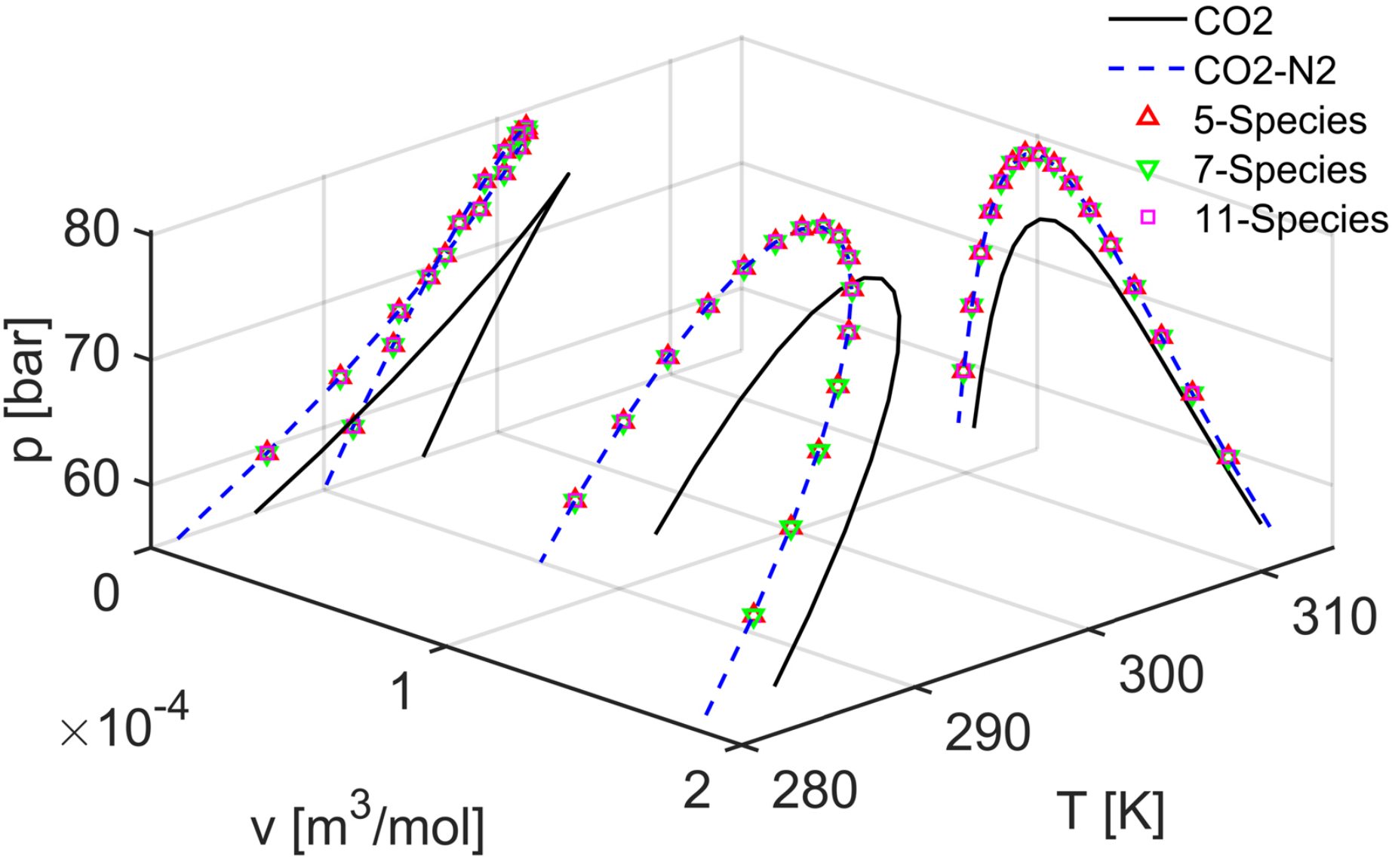
CO2
CO2-N2
5-Species
7-Species
11-Species
80
70
60
p [bar]
0
1
2
×10-4
v [m3/mol]
280
290
300
310
T [K]

Figure 1

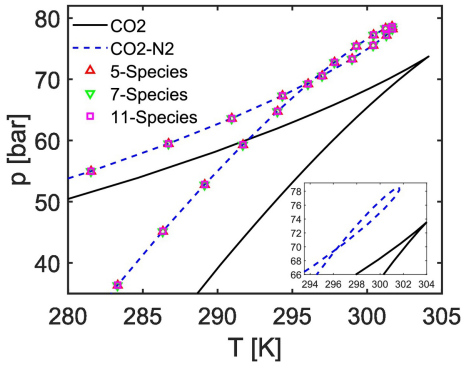
CO2
CO2-N2
5-Species
7-Species
11-Species
p [bar]
T [K]
80
70
60
50
40
280
285
290
295
300
305
78
76
74
72
70
68
66
294
296
298
300
302
304

a

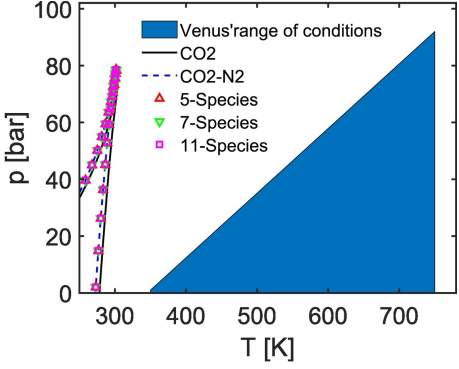
Venus'range of conditions
CO2
CO2-N2
5-Species
7-Species
11-Species
p [bar]
T [K]
100
80
60
40
20
0
300
400
500
600
700

b

Figure 2

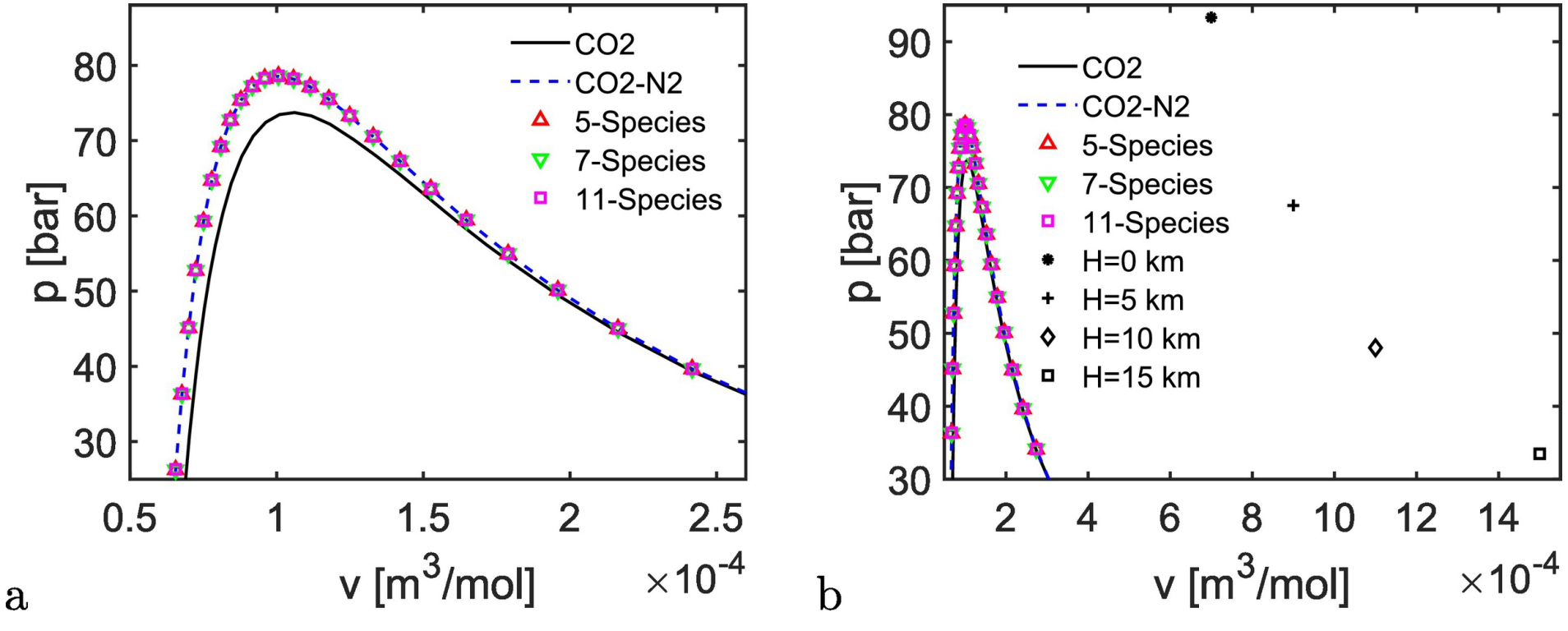
CO2
CO2-N2
5-Species
7-Species
11-Species
H=0 km
H=5 km
H=10 km
H=15 km
p [bar]
v [m3/mol]
×10-4
a
b

Figure 3

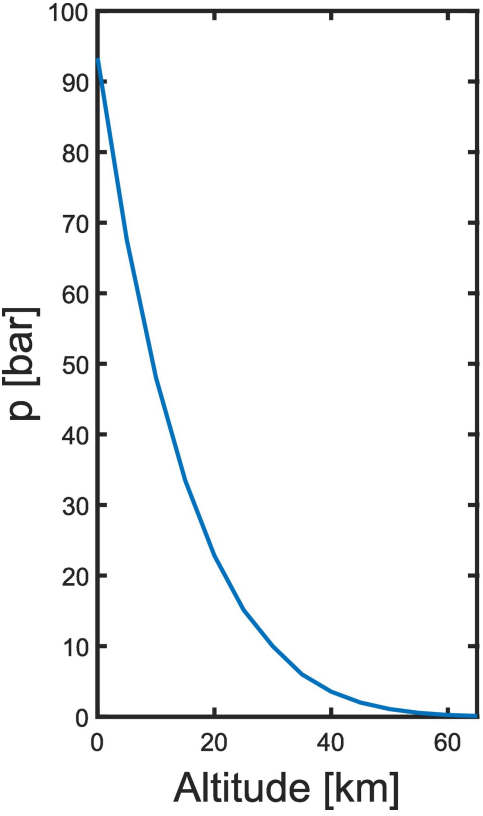
p [bar]
100
90
80
70
60
50
40
30
20
10
0
0
20
40
60
Altitude [km]

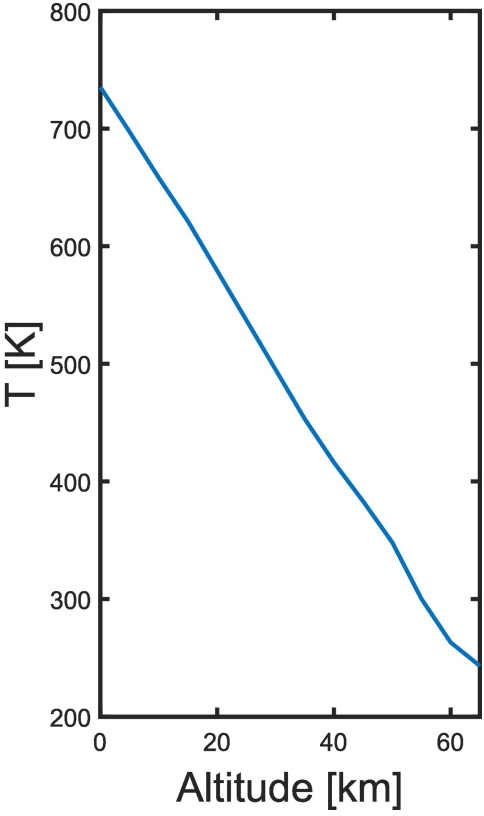
T [K]
800
700
600
500
400
300
200
0
20
40
60
Altitude [km]

Figure 4

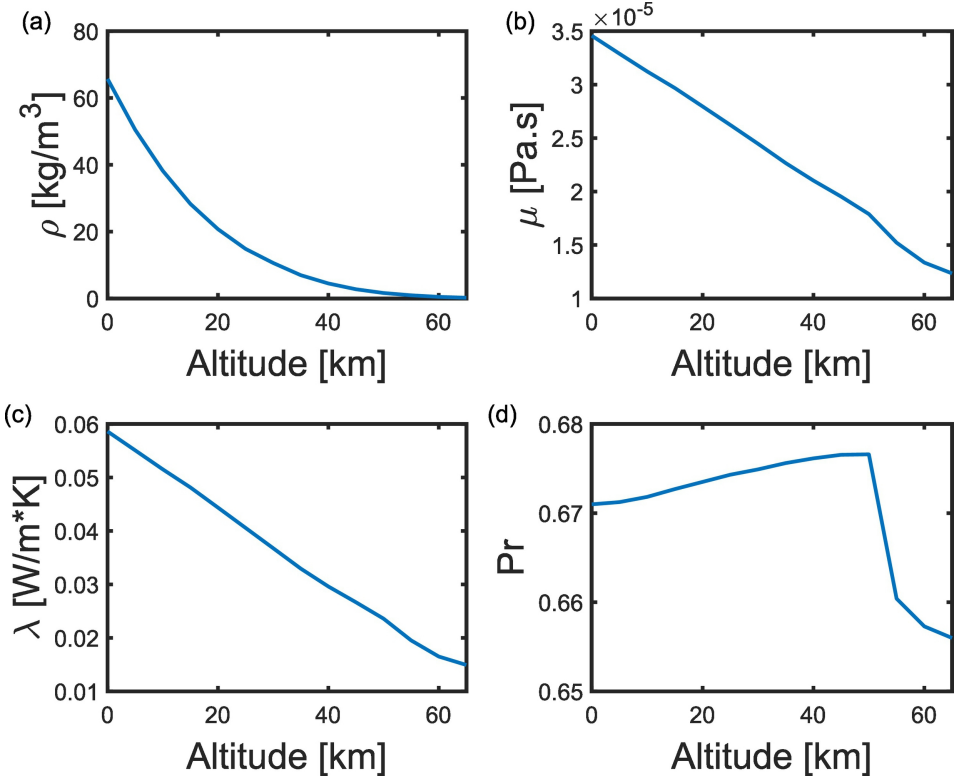
(a)
80
60
40
20
0
ρ [kg/m^3]
0
20
40
60
Altitude [km]
(b)
$\times 10^{-5}$
3.5
3
2.5
2
1.5
1
μ [Pa.s]
0
20
40
60
Altitude [km]
(c)
0.06
0.05
0.04
0.03
0.02
0.01
λ [W/m*K]
0
20
40
60
Altitude [km]
(d)
0.68
0.67
0.66
0.65
Pr
0
20
40
60
Altitude [km]

Figure 5

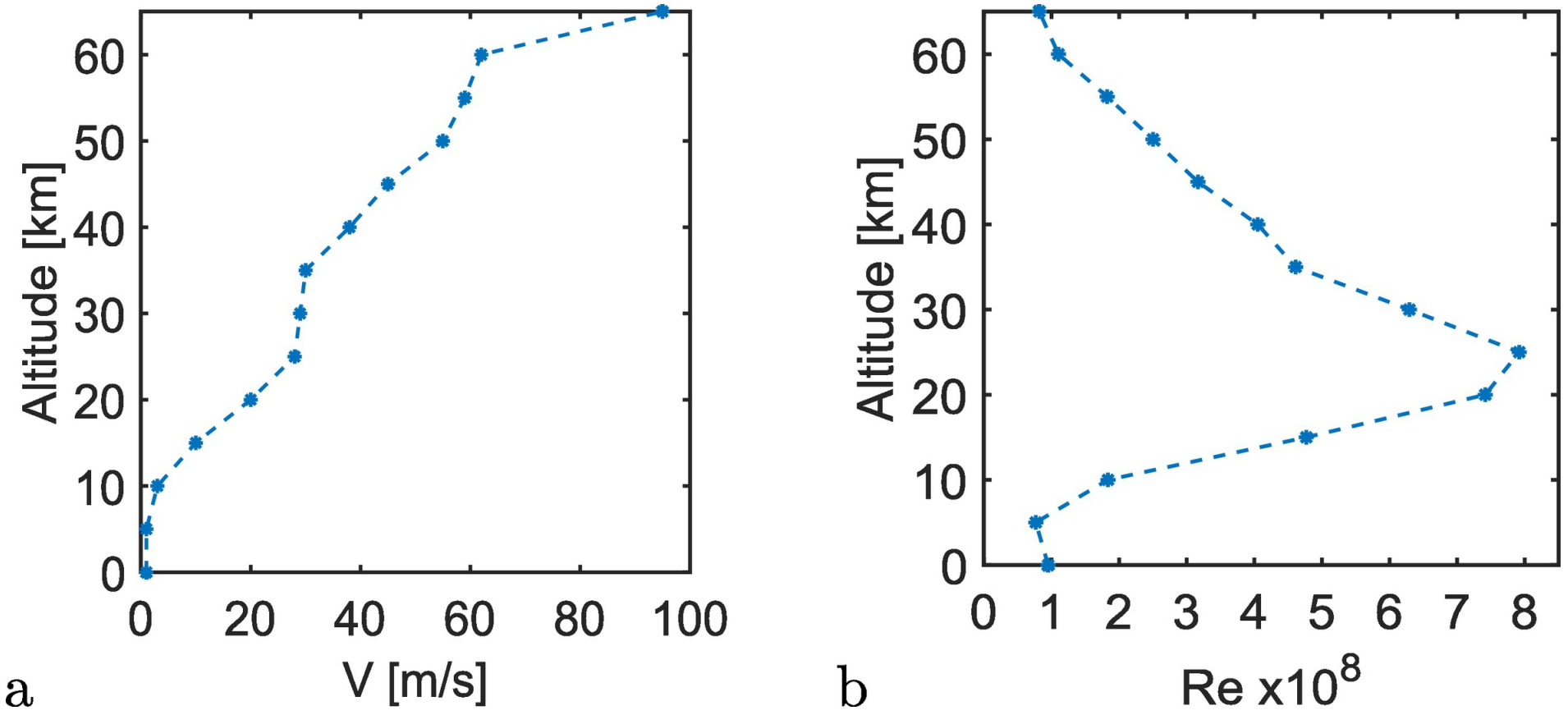
Altitude [km]
0
10
20
30
40
50
60
0
20
40
60
80
100
V [m/s]
a
Altitude [km]
0
10
20
30
40
50
60
0
1
2
3
4
5
6
7
8
Re x10^8
b

Figure 6

a

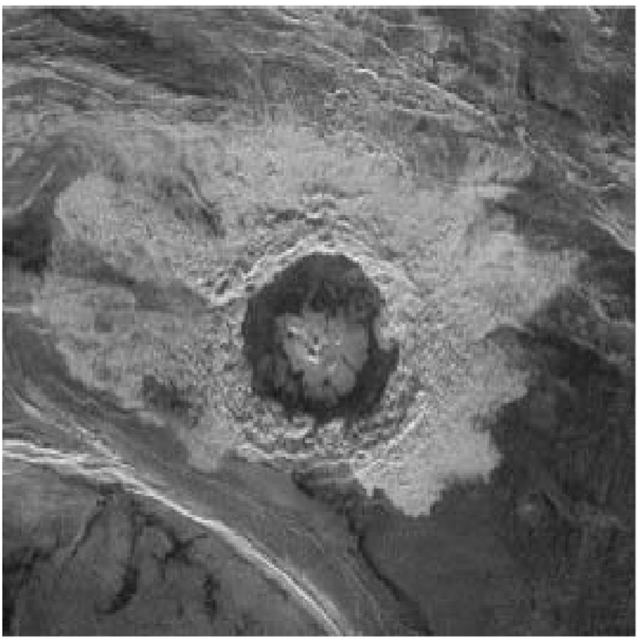

b

Figure 7

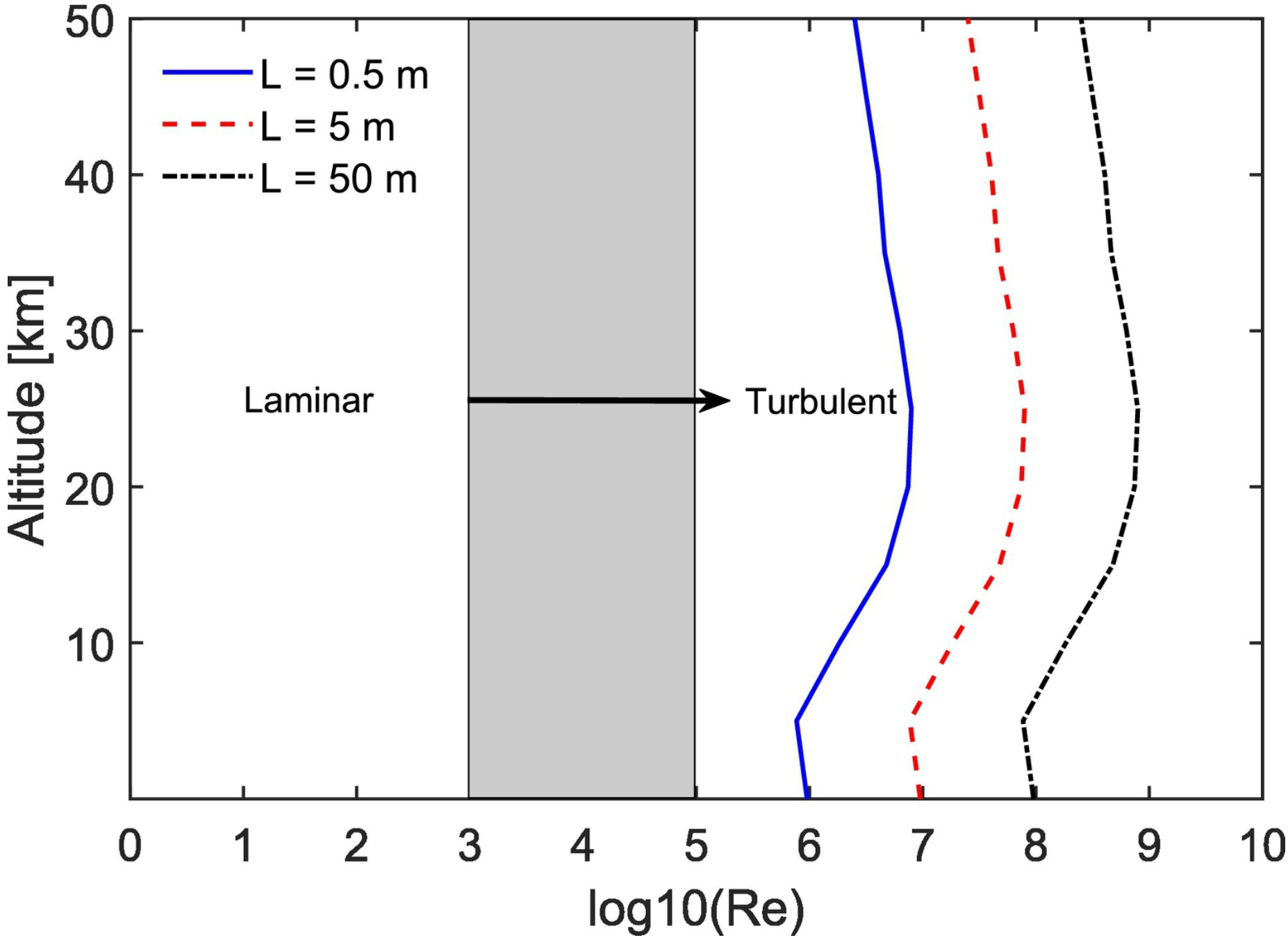
L = 0.5 m
L = 5 m
L = 50 m
Laminar
Turbulent
Altitude [km]
log10(Re)
50
40
30
20
10
0
1
2
3
4
5
6
7
8
9
10

Figure 8

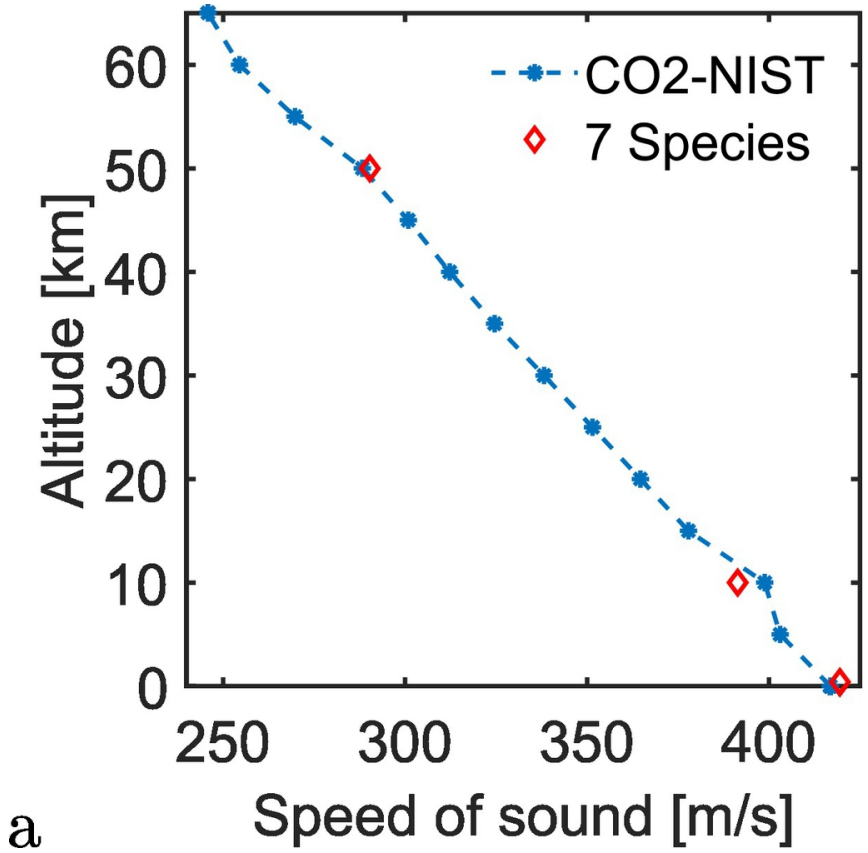
CO2-NIST
7 Species
Altitude [km]
Speed of sound [m/s]
0
10
20
30
40
50
60
250
300
350
400

a

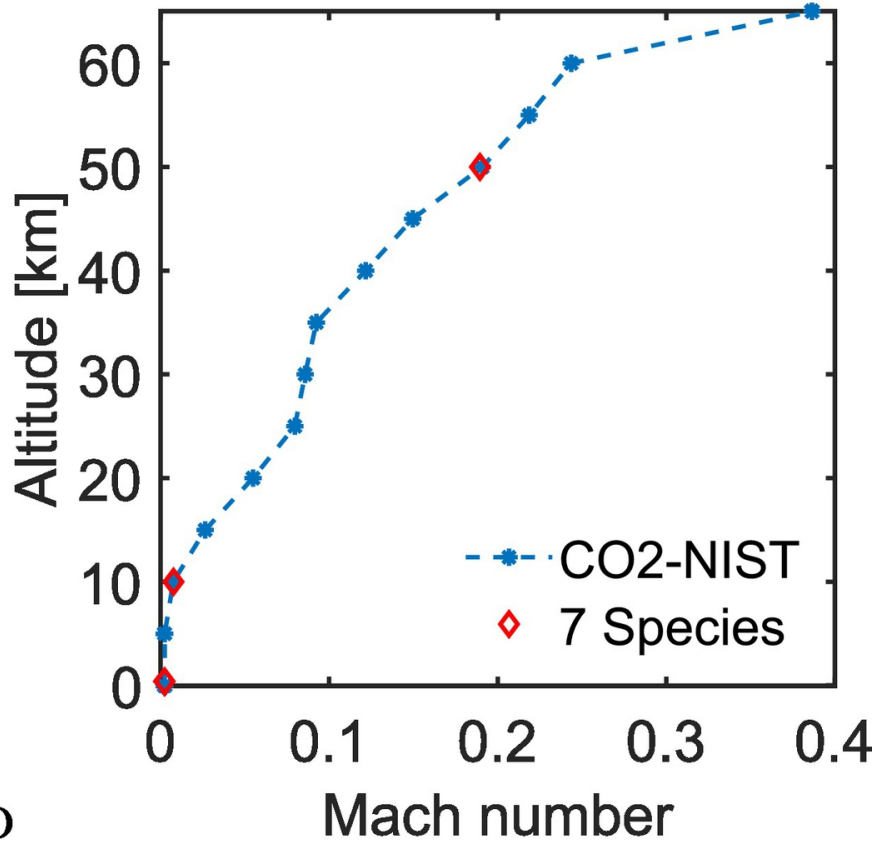
CO2-NIST
7 Species
Altitude [km]
Mach number
0
10
20
30
40
50
60
0
0.1
0.2
0.3
0.4

b

Figure 9